SYED MUBASHAR H. GARDAZI[1], JEHANZEB ALI SHAH[1], TAYYAB ASHFAQ[2],
TAUQIR A. SHERAZI[3], MUHAMMAD ARIF ALI[4], ARSHID PERVEZ[1],
NAIM RASHID[5], JAVED IQBAL[4], BILAL AHMAD ZAFAR AMIN[1], MUHAMMAD BILAL[1]

EQUILIBRIUM, KINETICS AND THERMODYNAMIC STUDY OF THE ADSORPTIVE REMOVAL OF METHYLENE BLUE FROM INDUSTRIAL WASTEWATER BY WHITE CEDAR SAWDUST

The study evaluated the adsorption potential of white cedar sawdust (WCS) for dye removal. WCS was chosen from five preferred, abundant waste biomasses from Pakistan. Various parameters such as contact time, adsorbent dose, dye concentration, pH, and particle size were optimized for methylene blue (MB) dye adsorption. The adsorbent was characterized by FTIR, SEM, EDX and BET analyses. The surface area of the adsorbent was $1.43 \text{ m}^2 \cdot \text{g}^{-1}$ and pore volume was $0.000687 \text{ cm}^3 \cdot \text{g}^{-1}$. The adsorption data best fitted the isotherm models of Langmuir, Temkin, Dubinin–Radushkevich, and Freundlich. The maximum experimental adsorption capacity obtained was $55.15 \text{ mg} \cdot \text{g}^{-1}$, which was in close agreement to the calculated adsorption capacity. Fitness of the pseudo-second order kinetics suggested chemisorption as the rate-limiting step. Thermodynamic study for adsorption was carried out to evaluate the Gibbs free energy ($\Delta G°$), enthalpy ($\Delta H°$) and entropy ($\Delta S°$). The negative values $\Delta G°$ at the examined temperature range confirmed the spontaneous adsorption of MB onto WCS.

1. INTRODUCTION

Industrial effluents contaminated with dyes pose a serious threat to fresh water bodies, the environment and human health. Methylene blue (MB) is one of the most frequently used dyes in textile industries, especially in the acrylic, silk, wool and cotton

---

[1]Department of Environmental Science, COMSATS University Islamabad, Abbottabad Campus, University Road, Abbottabad, 22060, KPK, Pakistan, corresponding author M. Bilal, e-mail address: mbilal@cuiatd.edu.pk

[2]Department of Civil Engineering, University of Hail, Hail Province, Saudi Arabia.

[3]Department of Chemistry, COMSATS University Islamabad, Abbottabad Campus, University Road, Abbottabad, 22060, KPK, Pakistan.

[4]Department of Soil Science, Faculty of Agricultural Science and Technology, Bahauddin Zakariya University, 60000, Multan.

[5]Department of Chemical Engineering, COMSATS Institute of Information Technology, Defense Road, Lahore, Pakistan.

dying [1]. Water containing MB causes serious impairments of the photosynthetic activity in plants and mutagenicity in animals. Moreover, it may cause allergic dermatitis skin irritation, diarrhea, cancer and mutation as well as eye burns, which may lead to permanent injury in human and animals [2]. On inhalation, it gives rise to rapid and difficult breathing, while ingestion produces burning sensation, nausea, vomiting, profuse sweating, mental confusion, and methemoglobinemia. Therefore, considering the hazardous environmental effects of MB, it is important to ensure the compliance with environmental regulations.

During the past few decades, several techniques have been used for decolorization and treatment of textile wastewater. Various methods for dye removal such as adsorption, precipitation, flocculation, ion exchange, electrokinetic coagulation, and ozonation have been investigated. However, the adsorption is an efficient method because of its design simplicity, ease of operation and insensitivity to toxic substances. Although commercial activated carbon is the preferred adsorbent for the dye removal due to its extended surface area, microporous structure and high adsorption capacity, yet its widespread use is restricted due to its elevated capital and regeneration cost. Therefore, efforts are being made to explore the inexpensive alternate bioadsorbents.

A number of low-cost adsorbents have been studied, offering treatment potential for dye removal, comparable to commercial activated carbon. The agricultural and forest wastes are mainly composed of lignocellulosic material including high molecular weight components, i.e., lignin, hemicellulose and cellulose. They also contain some low molecular size extractive structural components, which make them a good choice for the removal of different dyes. Efforts for the removal of MB have been made using waste grass biomass [3], cater seed shells, loofah plant [4], cherry, walnut, oak and pitch pine [5], rice husk, cotton waste, tomato plants roots, guava leaf powder, rattan sawdust activated carbon, neem leaf powder, papaya seeds [6–8]. Different untreated waste from agriculture and forest sectors can be a subject for intensive research, especially for dye and metal removal where they show high efficiency [9].

In this study, low-cost white cedar sawdust (WCS), was explored for MB removal potential in batch mode. Different process parameters such as contact time, initial dye concentration, temperature, pH, particle size, and adsorbent doses were optimized. The mechanisms and adsorptive nature of the WCS during the adsorption process were studied using isotherm, kinetic models and thermodynamic.

2. MATERIALS AND METHODS

Waste biomasses, i.e., peanut shells, tobacco stalks, hemp leaves, cedar seeds, white cedar sawdust (WCS), were collected from Khyber Pakhtunkhwa province, Pakistan. The adsorbents were washed with deionized water, dried, grounded, and sieved for required mesh sizes. Analytical grade (C.I. 52015 Merck, Germany) methylene blue (MB)

dye was used as a reagent. The stock solution of 1000 mg·dm^{-3} was prepared by dissolving 1 g of dye in 1000 cm^3 of deionized water. All working solutions were prepared by diluting the stock solution with deionized water. The absorbance measurements were taken on UV-Vis spectrophotometer (PG 80$^+$ UK) at the maximum wavelength of 668 nm in dependence on pH of the solutions (Fig. 1). Therefore, to assess the influence of pH on MB adsorption by WCS adsorbent, a new calibration curve was developed for the respective pH value.
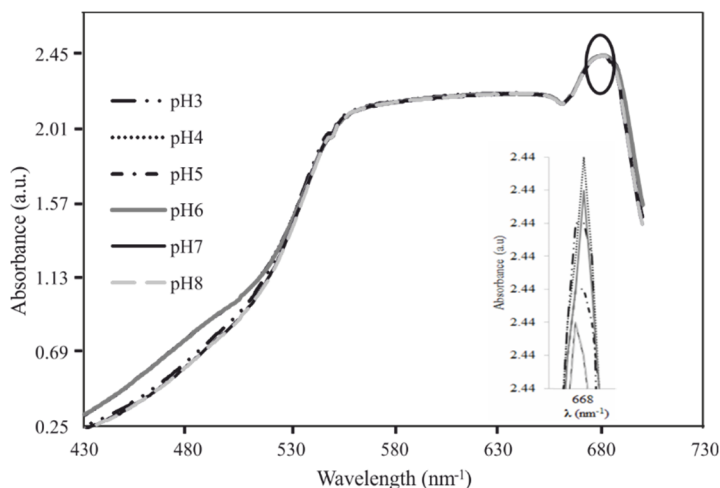

Fig. 1. Dependences of absorbance on the absorption wavelength λ
for various pH

Batch adsorption experiments were performed in conical flasks of 100 cm^3 in temperature-controlled orbital shaking incubator at 220 rpm and 30 °C. 0.05 g of the adsorbent was added to 50 cm^3 of the solution with an initial dye concentration of 50 mg·dm^{-3}. After shaking for a particular time, the adsorbent was separated from the solution by centrifugation at 4000 rpm for 10 min and filtered through 0.45 µm cellulose nitrate filter paper. All the waste adsorbents were screened for their MB adsorption potential. Afterwards, the adsorbent possessing the highest efficiency was subjected to further investigation, and the experimental conditions were optimized. The equilibrium distribution of dye between adsorbent and the aqueous solution was recorded for 240 min. The effects of operational and environmental parameters on removal capacity of the adsorbent were examined till reaching equilibrium. These parameters include pH (3–8), temperature (30–50 °C), initial adsorbate concentration (30–300 mg·dm^{-3}), particle size (105–400 µm) and the amount of adsorbent (0.1–5 g·dm^{-3}). The pH of the solution was adjusted with 0.1 M HCl and 0.1 M NaOH solutions and was measured with a pH meter (PHS-25CW, Shanghai). The amount of MB adsorbed (q_t, Eq. (1)) at time t, equilibrium adsorption

capacity (q_e, Eq. (2)) and the sorption efficiency (S, Eq. (3)) of the adsorbent were calculated as follows:

$$q_t = \left(\frac{C_0 - C_t}{m} \right) V \tag{1}$$

$$q_e = \left(\frac{C_0 - C_e}{m} \right) V \tag{2}$$

$$S = \left(\frac{C_0 - C_t}{C_0} \right) \times 100\% \tag{3}$$

where q_e is the amount of MB adsorbed by 1 g of adsorbent (mg·g^{-1}), at equilibrium. C_0, C_t and C_e were initial, residual concentrations of MB (mg·dm^{-3}) in the solution at any time and at equilibrium, respectively. m and V are the mass of adsorbent (g) and volume of the solution (dm^{-3}), respectively. Both the adsorption capacity and sorption efficiency are important parameters in comparing performance of various adsorbents. Adsorption capacity gives us an idea about the amount of contaminant which can be carried by a unit mass of adsorbent while sorption efficiency is just the removal efficiency of adsorbent irrespective of its amount.

pH at the point of zero charge (pH$_{zpc}$) for the studied adsorbent was determined by the salt additions. For this purpose, 0.5 g of WCS was added to 50 cm^3 of 0.1 M NaCl solution in 100 cm^3 conical flasks. Initial pH (pH$_i$) of the solution (3–8) was adjusted with 0.1 M HCl and 0.1 M NaOH solutions. These samples were shaken for 4 h in a temperature-controlled orbital shaker at 220 rpm and 30 °C. Afterwards, the final pH (pH$_f$) of the solution was measured. Change in pH (ΔpH) was plotted against the pH$_i$ and thereafter, pH$_{zpc}$ was determined at ΔpH = 0.

The Langmuir, Temkin, Dubinin–Radushkevich (D–R), and Freundlich isotherms and pseudo-first and pseudo-second order kinetic models were applied to explain the mechanism of MB adsorption onto the WCS. The corresponding constants and correlations of the model plots were calculated. Moreover, spontaneity and randomness at the solid–liquid interface were investigated through a thermodynamic study.

WCS adsorbent was characterized using the Fourier transform infrared spectroscopy (FTIR), Brunauer, Emmett and Teller (BET) model, scanning electron microscopy (SEM) and energy-dispersive X-ray spectroscopy (EDX) before and after dye adsorption. FTIR analysis of WCS was carried out to elucidate the possible functional groups that may participate in adsorption process of MB. The dried adsorbent (before and after MB adsorption) was converted into pallets using KBr and then FTIR spectrum was recorded. BET analysis of WCS adsorbent was performed under the set conditions, i.e., pressure 0.05–0.3 $p/p°$, temperature 77.03 K and warm free space of 9.9562 cm^3. SEM

analysis was performed to study the morphology of the adsorbent material. The samples were mounted on brass stubs using double-sided adhesive tape. SEM photographs were taken with scanning electron microscope (HITACHI S-3000N, JAPAN) at magnification 350× and 1500×. The working distance of 25 mm was maintained and the images were collected at acceleration voltage of 20 kV while using secondary electron detector.

All the measurements reported in the present study are average values of multiple (at least three) independent measurements. Statistical analysis was carried out by computer software Statistica Statsoft 10. The whole data were subjected to one-way analysis of variance (ANOVA), and differences were considered significant at $p = 0.01$.

3. RESULTS AND DISCUSSION

Selection of an efficient adsorbent for MB removal was done through batch screening of five different adsorbents. It is shown in Fig. 2 that among five different adsorbents, the WCS has significant ($p = 0.01$) higher adsorption capacity, i.e., 41.4 mg·g^{-1}, with better sorption efficiency (82.8%), compare to others such as peanut shells (27.4 mg·g^{-1}, 54.8%), tobacco stalks (30.2 mg·g^{-1}, 60.4%), hemp leaves (32.4 mg·g^{-1}, 64.8%), cedar seeds (33.8 mg·g^{-1}, 67.6%). According to these results, WCS was ranked as an efficient adsorbent, so selected for further investigation to optimize environmental conditions to obtain the maximum MB adsorption.
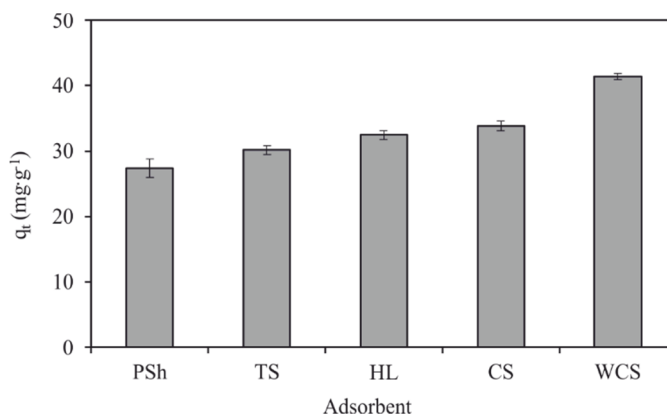

Fig. 2. Screening of the adsorption potential of pea nutshells (PSh), tobacco stalks (TS), hemp leaves (HL), cedar seeds (CS), white cedar sawdust (WCS) for MB removal. Contact time 24 h, C_0 50 mg·dm^{-3}, adsorbent dose 1 g·dm^{-3}, pH 6, temperature 303 K, particle size 400 µm

Functional groups at WCS adsorbent were determined by FTIR analysis. This is of vital importance to understand the adsorption phenomena particularly when it is chemisorption. Figure 3 presents the FTIR spectrum of WCS adsorbent, before and after adsorption of

MB. The characteristic peak due to C–C stretching bond in organic adsorbent appeared at 2925 cm^{-1} which also appeared in the sample after adsorption. The peaks at 1630 cm^{-1} and 1385 cm^{-1} are attributed to vibration of carbon to carbon double bond (C = C) and N–H bending, respectively.
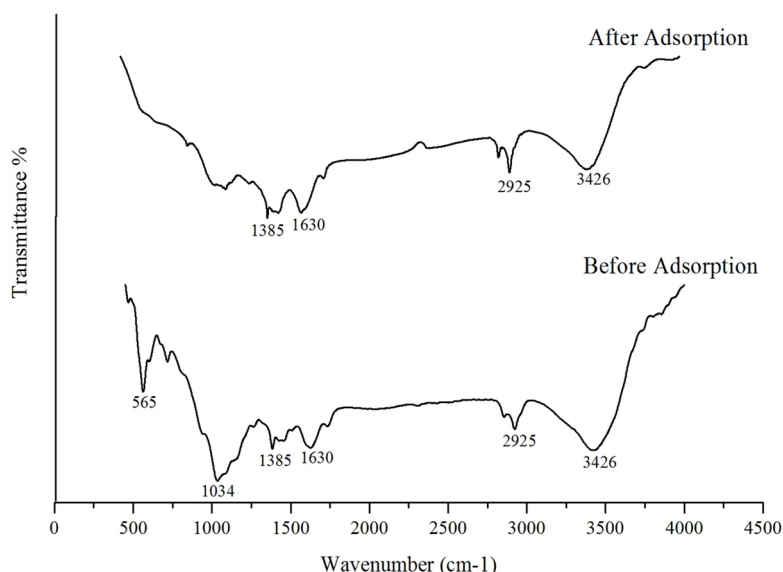

Fig. 3. FTIR analysis of WCS adsorbent surface

The appearance of a broad peak at 3426 cm^{-1} is due to O–H stretching mode indicating the presence of alcoholic and hydrogen-bonded water in the cell wall of biomass. These alcoholic groups may be responsible for chemisorption of MB, enhancing the overall adsorption yield. The elemental analysis of WCS adsorbent indicated the presence of silicon, which also confirmed through FTIR peak at 1034 cm^{-1} and is attributed to Si–O stretching. Moreover, the absorption at 1034 cm^{-1} may also be attributed to C–O stretching in ethers (–C–O–C–) [10], methoxy group (O–CH$_3$) and in aminated epoxy-lignin (C–OH) [11], and methylene linkages (N–CH$_2$–N) in an organic compound derived from wood (furfural) [12]. The peak at 565 cm^{-1} was assigned to C–H bending as reported in vegetable wastes activated carbon as well as to chloro-alkane groups [13]. The disappearance of peaks at 1034 cm^{-1} and 565 cm^{-1} ratified their indisputable participation of functional groups (O–H, O–CH$_3$, C–O, C–OH, C–H,) during MB adsorption.

According to BET analysis, the surface area of the WCS was 1.4302 m^2·g^{-1} with single point adsorption (assuming BET intercept equal to zero) and total pore volume was found to be 0.000687 cm^3·g^{-1}. The adsorbent average pore width (4 V/A by BET) was found as 192 nm. The particle size of WCS can affect its adsorption property. The

average particle size of the WCS adsorbent (4.12 µm) suggested a high surface area which would be exposed to MB adsorption.

The morphological analysis of WCS adsorbent was carried out through SEM (Fig. 4). The images were captured at a magnification of 350× and 1500×. These images reflected the porous structure of WCS adsorbent where the primary and secondary pores were identified, supporting the adsorption phenomenon. Although the secondary pores were found in the range of 0.5–2 µm, yet the high removal of MB (85–98%) revealed the presence of perhaps tertiary pores inside the secondary pores which were not captured in SEM photographs. In Table 1, the results of the EDX analysis have been presented, revealing the presence of various elements, mainly C (43.95%), O (42.51%), Mg (9.12), Si (1.71%), K (1.39%) and Ca (1.33%) in the WCS adsorbent.
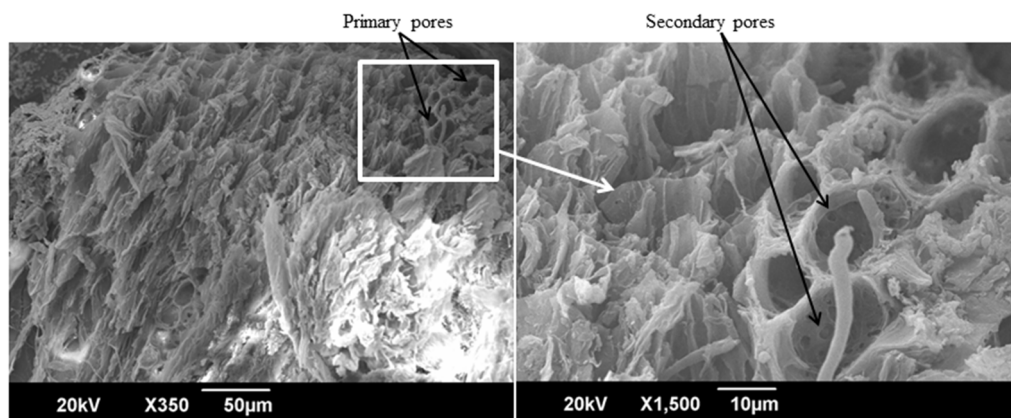

Fig. 4. SEM images of WCS adsorbent before MB adsorption

Table 1

EDX-quantitative analysis of the WCS adsorbent

Element	E [keV]	Weight per cent	Atom per cent
C	0.277	43.95	53.65
O	0.525	42.51	38.96
Mg	1.253	9.12	5.5
Si	1.739	1.71	0.89
K	3.312	1.39	0.52
Ca	3.69	1.33	0.49

The effect of contact time on the adsorption of MB on WCS has been evaluated as shown in Fig. 5a. The contact time of 240 min is sufficient to achieve the equilibrium adsorption, i.e., $q_e = 39$ mg·g^{-1} which is equivalent to ca. 80% adsorption. Further increase in contact time did not significantly ($p = 0.01$) changed the adsorption even upon

extending time up to 24 h. Therefore the remaining batch experiments were carried within the assumed time of 240 min to reach equilibrium. The rapid initial adsorption and gradual decrease with increasing time are attributed to the abundant availability of the active sites on the adsorbent surface during the initial 60 min of batch adsorption. Afterwards, the remaining vacant sites become difficult to be occupied due to the fact that the dye molecules on the surface of adsorbent repel those present in the aqueous solution, resulting in the decrease of dye adsorption onto the adsorbent.
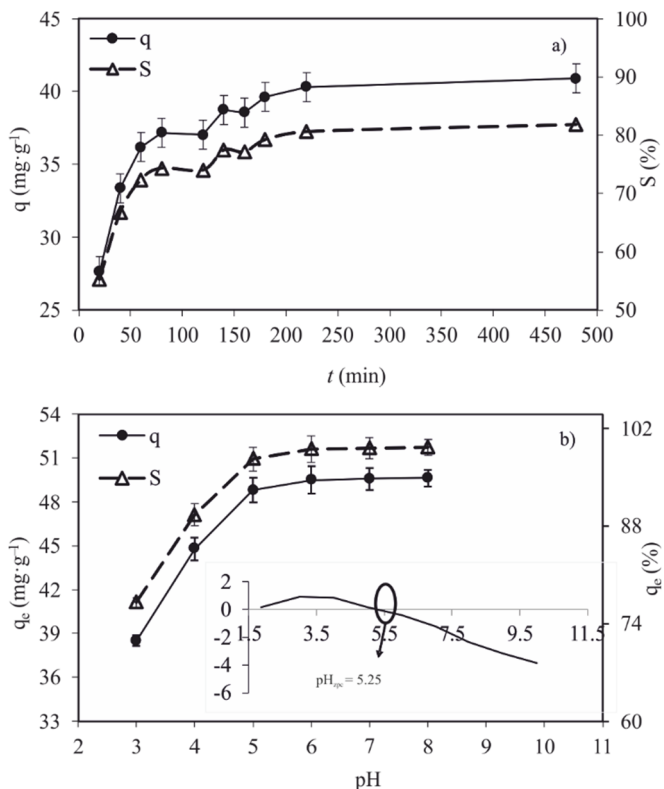

Fig. 5. Effect of a) contact time at pH 6 and b) pH (contact time 240 min) onto the MB adsorption of WCS; C_0 50 mg·dm^{-3}, adsorbent dose 1 g·dm^{-3}, temperature 303 K, particle size 400 μm

MB is a cationic dye, which exists in the aqueous solution in the form of positively charged ions. Being an ionic species, the degree of its adsorption onto the WCS surface is primarily influenced by the surface charge on the adsorbent, which in turn is influenced by pH (Fig. 5b). MB adsorption onto WCS adsorbent was significantly ($p = 0.01$) lower at pH 3 (38.50 mg·g^{-1}) than at pH 5–8 (48.80–49.30 mg·g^{-1}). The excess of H$^+$ ions may compete with the cation groups of MB for active adsorption sites. Moreover, at high pH, the positive charges at the solid–liquid interface decrease and the adsorbent

surface becomes negatively charged. pH_{zpc} was found 5.25. Therefore, the MB adsorption by WCS is favored at $pH > pH_{zpc}$. In contrast, at a low pH and $pH < pH_{zpc}$, the positive charge on the solid–liquid interface increases, and dominates onto the adsorbent surface, consequently, MB adsorption is decreases.
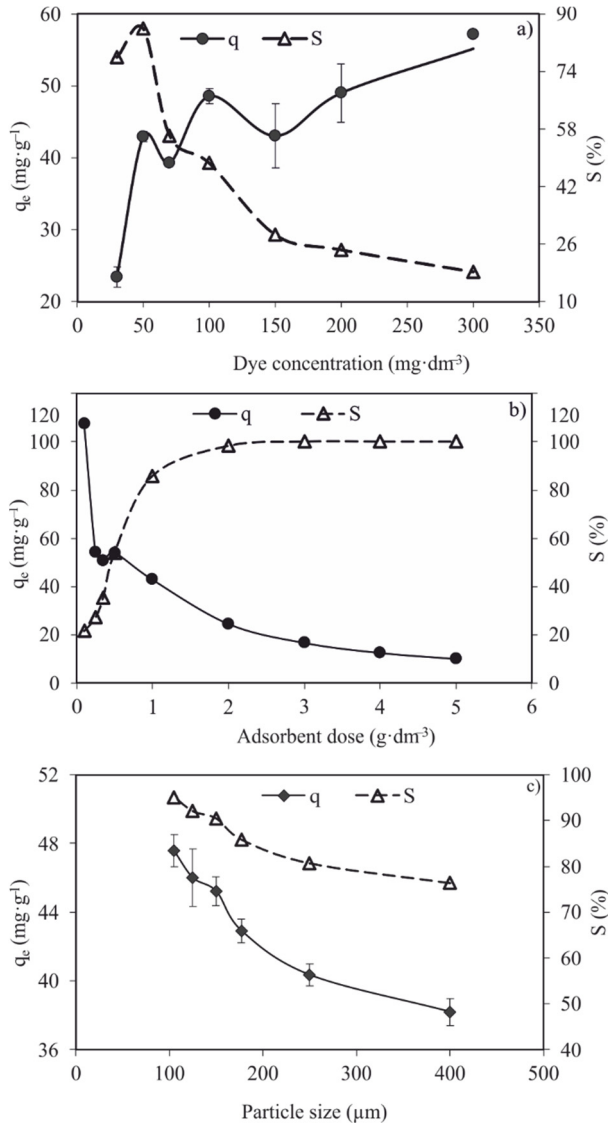

Fig. 6. Effect of initial dye concentration (a), adsorbent dose (b), and particle size (c) on the MB adsorption capacity of WCS; parameters constant in particular experiments: pH 6, temperature 303 K, contact time 240 min, C_0 50 mg·dm^{-3} (excluding a), adsorbent dose 1 g·dm^{-3} (excluding b), particle size 400 µm (excluding c)

The MB adsorption capacity of WCS increased from 23.39 to 55.15 mg·g^{-1} with increasing the initial dye concentration from 30 to 300 mg·dm^{-3} (Fig. 6a). This is probably due to a high-mass transfer driving force due to which adsorption sites previously inaccessible became available. However, the percentage removal of dye decreased from 77.98 to 18.38% with the given increase of initial dye concentration, which was expected due to the saturation of active binding sites of the WCS adsorbent. This is because increase in number of dye molecules was much larger compared to corresponding increase in the number of available adsorption sites; hence there was a net decrease in the removal efficiency or sorption efficiency.

The sorption efficiency of WCS increased from 21.5 to 100% upon the incremental increase in adsorbent dose from 0.1 to 5.0 g·dm^{-3}, respectively (Fig. 6b). This is due to the availability of more active sites and increased surface area of a greater amount of adsorbent. However, the adsorption of MB per unit mass decreased significantly ($p = 0.01$) from 107.51 to 10.01 mg·g^{-1} by increasing the WCS dose from 0.1 to 5.0 g·dm^{-3}. This can be attributed to partial overlapping or aggregation at higher adsorbent dose, which results in a decrease in total surface area and active sorption sites. Moreover, data did not reflect any significant ($p = 0.01$) MB removal (16. 67–10.01 mg·g^{-1}) at the WCS dose from 3.0 to 5.0 g·dm^{-3}, which may be ascribed to the higher number of unsaturated active binding sites during the bio-adsorption process [14, 15].

The particle size of an adsorbent could be one of the important factors affecting its sorption efficiency. Data in Fig. 6c revealed significant ($p = 0.01$) decrease in MB adsorption (from 48 to 38 mg·g^{-1}) with an increased particle size of the WCS, i.e., from 105 to 400 µm. This is due to the fact that a decrease in particle size leads to an increase in the total surface area while keeping the total amount constant. Besides, smaller particle size provides better accessibility of MB molecules into secondary and tertiary pores (Fig. 4) during the adsorption process. Moreover, a higher number of active pores have been observed in small particle size of adsorbent than large particles, which increase the dye uptake capacity. This is because the diffusion resistance to mass transport from larger particles is higher, and most of the internal surface of the particle may not be utilized for adsorption. Consequently, the amount of adsorbed MB decreases.

Various isotherm models, i.e., Langmuir [16], Freundlich [17], Dubinin–Radush-kevich (D–R) [18], Temkin [19] were used to elucidate the nature and optimization of the studied adsorption system (Table 2). Langmuir isotherm assumes the homogeneous distribution of active sites at the surface of an adsorbent, and there are no significant interactions between adsorbed species. The linear form of Langmuir isotherm applied to adsorption data is as follows

$$\frac{C_e}{q_e} = \frac{1}{K_L q_{max}} + \frac{C_e}{q_{max}} \tag{4}$$

where q_{max} is the maximum Langmuir adsorption capacity (mg·g^{-1}), and K_L is the Langmuir constant (dm^3·mg^{-1}) calculated from slope and intercept of the plot (Fig. 7a).

T a b l e 2

Adsorption isotherms constants

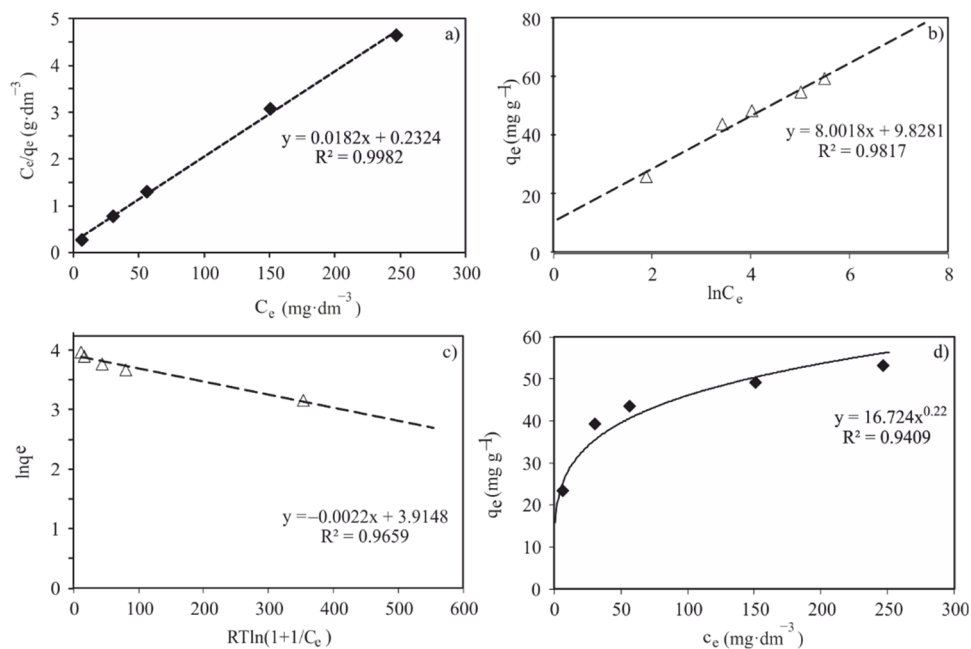| Isotherm	Parameter	Value
Langmuir	$q_{e\,exp}$, mg·g^{-1}	55.15
	q_{max}, mg·g^{-1}	54.94
	K_L, dm^3·mg^{-1}	0.078
	R^2	0.998
Temkin	A_T, dm^3·g^{-1}	3.415
	b_T, kJ·mol^{-1}	314.98
	R^2	0.982
Freundlich	$1/n$	0.22
	N	4.55
	K_f, dm^3·g^{-1}	16.22
	R^2	0.9986
Dubinin–Radushkevich	q_{DR}, mg·g^{-1}	50.14
	B, mol^2·kJ^{-2}	0.0011
	E, kJ·mol^{-1}	21.32
	R^2	0.9659

Fig. 7. Langmuir (a), Temkin (b), Dubinin–Radushkevich (c), and Freundlich (d) isotherms

The Langmuir isotherm model reflected the best fit ($R^2 = 0.998$) to the adsorption data. The closeness of $q_{e\,exp}$ (experimental adsorption capacity) and q_{max} confirmed the applicability of the Langmuir model (Table 2). The Langmuir constant K_L depends on

the binding energy between adsorbate and adsorbent. The validity of Langmuir isotherm can also be proved through a dimensionless constant, the equilibrium parameter RL (separation factor, Eq. (5)), which measures the suitability of WCS adsorbent for removal of the MB.

$$R_L = \frac{1}{1 + K_L C_0} \tag{5}$$

Adsorption of any pollutant is regarded favorable, if $0 < RL < 1$, whereas unfavorable if $RL > 1$, linear if $RL = 1$, and irreversible if $RL = 0$. In the present study, RL was found to be 0.11, showing that WCS is a useful material for the adsorption of MB. It also indicated the formation of a monolayer of adsorbate molecules, which may saturate the homogeneous surface of the WCS adsorbent.

Temkin isotherm model postulates: (i) heat of adsorption of all the molecules in the layer decrease linearly rather than logarithmically with coverage [20]; and (ii) adsorption phenomenon is characterized by a uniform distribution of binding energies at the surface of an adsorbent [19, 21]

$$q_e = \frac{RT}{b_T} \ln\left(A_T C_e\right) \tag{6}$$

$$B = \frac{RT}{b_T} \tag{7}$$

$$q_e = B \ln A_T + B \ln C_e \tag{8}$$

In Equations (6)–(8), A_T (dm^3·g^{-1}) is the equilibrium binding constant, B (kJ·mol^{-1}) is the constant related to adsorption energy, b_T is the Temkin isotherm constant, T and R are the absolute temperature (K) and universal gas constant (8.314 J·mol^{-1}·K^{-1}). The constants A_T and b_T were calculated from the plot q_e vs. lnC_e. Temkin model indicated the good fit to the adsorption data with the R^2 value of 0.9817 (Fig. 7b, Table 2). Fitness of this model with the data suggests the uniform surface energies of the WCS. The R^2 value was also nearer to that of Langmuir, and higher than Freundlich, which reveals the homogeneity of the adsorbent surface.

Equilibrium data were also modeled by Dubinin–Radushkevich isotherm:

$$\ln q_e = \ln q_{DR} - \beta \varepsilon^2 \tag{9}$$

q_{DR} is the theoretical monolayer sorption capacity (mg·g^{-1}) and β is the constant of adsorption energy (mol^2·K·J^{-2}), whereas ε is the Polanyi potential:

$$\varepsilon = RT \ln \left(1 + \frac{1}{C_e} \right) \tag{10}$$

It is observed from Fig. 7c that the R^2 value (0.9659) is lower than that of Langmuir, Freundlich and Temkin isotherm models. According to Table 2, the values of q_{DR} and β were 50.14 mg·g^{-1} and 0.0011 mol^2·kJ^{-2}, respectively. The mean free energy (E) required by one mole of adsorbate to reach the active sites from an infinite distance calculated from

$$E = \frac{1}{\sqrt{2\beta}} \tag{11}$$

is 21.32 kJ·mol^{-1}. Its value is quite large, but even so, it depicts the characteristics of chemisorption with an ion-exchange mechanism, i.e., 8–16 kJ·mol^{-1}. This shows the strong electrostatic interactions between the negatively charged surface of WCS adsorbent and cationic MB molecule (pH = 6).

Freundlich isotherm assumes the contaminant adsorption on the heterogeneous surface of the adsorbent:

$$q_e = K_F C_e^{1/n} \tag{12}$$

The constants K_F and $1/n$ are the relative adsorption capacity (16.7 dm^3·g^{-1}) and heterogeneity factor (0.22) (Table 2), which determine the intensity, and feasibility of the adsorption process, respectively. These constants were calculated from the plot of q_e vs. C_e. The value of $1/n$ (Freundlich exponent) should be less than 1 for the favorable adsorption [17, 22, 23]. In the present study, the value of $1/n$ was 0.22, which indicated the usefulness of WCS adsorbent for the adsorption of MB. However, Freundlich model (Fig. 7d) revealed poor fit ($R^2 = 0.9409$) to the equilibrium data as compared to Langmuir model which, in turn, reflected the homogeneous distribution of active sites and monolayer coverage of WCS.

Based on the coefficient of determination (R^2), MB adsorption equilibrium is best described by the Langmuir isotherm model for the entire adsorption system under the studied conditions.

The dependence of the adsorption capacity of WCS on the contact time is presented in Fig. 8. The binding of adsorbate to active sites of WCS requires relatively longer contact time. Adsorption reaction models originating from chemical reaction kinetics are based on the whole process of adsorption without considering the actual mechanism of contaminant transport. This is because analysis of adsorption rates is sufficient for practical operation and from a system design viewpoint. Two models were used to study

the adsorption kinetics of MB adsorption onto WCS, i.e., pseudo-first, and pseudo-second order reaction models.

Lagergren first-order model is the earliest one describing the adsorption rate based on the adsorption capacity

$$\log\left(q_e - q_t\right) = \log q_e - \frac{K_1 t}{2.303} \tag{13}$$

where q_t (mg·g^{-1}) is the amount of adsorbate adsorbed at time t and K_1 (min^{-1}) is the pseudo-first order rate constant. The driving force, $(q_e - q_t)$, is proportional to the available fraction of active sites. Values of the rate constant (K_1, 0.009–0.015 min^{-1}), equilibrium adsorption capacity (q_e, 9–78 mg·g^{-1}) and the correlation coefficients (R^2, 0.438–0.876) were calculated from the plot $\log(q_e - q_t)$ vs. t (Table 3). WCS did not reflect a strong correlation in the most cases which indicated that the film diffusion or mass transfer is not the primary rate-controlling process. Differences between experimental ($q_{e\,\exp}$) and calculated ($q_{e\,\text{cal}}$) values indicated that the adsorption kinetics of pseudo-first order model could not be reproduced.

Table 3

Pseudo-first order and pseudo-second order models for MB adsorption onto WCS

C_0 MB [mg·dm^{-3}]	Pseudo-first order				Pseudo-second order			
	$q_{e\,\exp}$ [mg·g^{-1}]	K_1 (min^{-1})	$q_{e\,\text{cal}}$ [mg·g^{-1}]	R^2	K_2 [g·mg^{-1}·min^{-1}]	$q_{e\,\text{cal}}$ [mg·g^{-1}]	H [mg·g^{-1}·min^{-1}]	R^2
30	24.7	0.011	11.23	0.876	0.0019	26.45	1.35	0.993
50	41.79	0.009	9.22	0.438	0.0021	42.37	3.84	0.997
70	44.26	0.011	11.79	0.566	0.0018	60.24	6.58	0.988

Pseudo-second order model (Eq. (14)) is based on the assumption that the rate-limiting step may be the chemisorption involving valence forces through sharing or exchange of electrons between sorbent and sorbate. It has been successfully applied to the adsorption of metal ions, dyes, herbicides, oils, and organic substances from aqueous solutions [23–25]. The pseudo-second-order has the following advantages: it does not have the problem of assigning an effective adsorption capacity, i.e., the adsorption capacity, the pseudo-second order rate constant , and the initial adsorption rate all can be determined from the equation without knowing any parameter beforehand.

$$\frac{1}{q_t} = \frac{1}{K_2 q_e^2} + \frac{t}{q_e} \tag{14}$$

K_2 (g·mg^{-1}·min^{-1}) is the pseudo-second order rate constant and the product of K_2 and q_e^2 is the initial adsorption rate and is represented by h (mg·g^{-1}·min^{-1}). Initial adsorption

rate (h) and rate constant (K_2), were determined from the intercept and the slope of the plot t/q_t vs. t. The R^2 values (0.993–0.988, Fig. 8) indicated that the adsorption of MB onto WCS obeyed the pseudo-second order model in contrast to pseudo-first order kinetic model. Moreover, a good agreement was observed between the calculated values with experimental ones (Table 3).
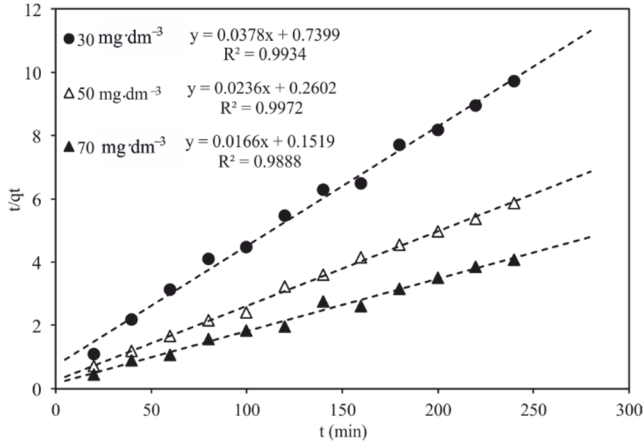

Fig. 8. Dependences of tq_t on time for MB adsorption onto WCS

The average relative error deviation (ARED) between experimental and theoretically calculated adsorption capacities was determined to verify the adequacy of pseudo-second order

$$\text{ARED} = \frac{1}{N}\sum\left(\frac{q_{e\,\text{cal}} - q_{e\,\text{exp}}}{q_{e\,\text{cal}}}\right)\times 100\% \tag{15}$$

where N is the number of data points during the kinetic experiment. The results showed 0.5–0.2% deviation along the increasing initial dye concentrations. The values of K_2 irregularly changed with increasing initial dye concentration, however, the fitness of the pseudo-second order model is the indication of chemisorption as the rate controlling step. Chemisorption involves the valence forces via sharing of electron or exchange between the adsorbent and adsorbate [26].

Thermodynamic parameters were calculated to further check the effect of temperature on MB adsorption onto WCS (Table 4). The equilibrium constant K_{eq} was calculated from

$$K_{eq} = \frac{q_e}{C_e} \tag{16}$$

where q_e is the adsorption capacity and C_e is the liquid phase concentration at equilibrium. Standard changes in enthalpy and entropy were calculated from van't Hoff equation (Fig. 9):

$$\ln K_{eq} = \frac{\Delta S^\circ}{R} - \frac{\Delta H^\circ}{RT} \tag{17}$$

where ΔH° (kJ·mol^{-1}) is a change in standard enthalpy, ΔS is a change in standard entropy (kJ·mol^{-1}·K^{-1}), K_{eq} is the equilibrium constant of adsorption.
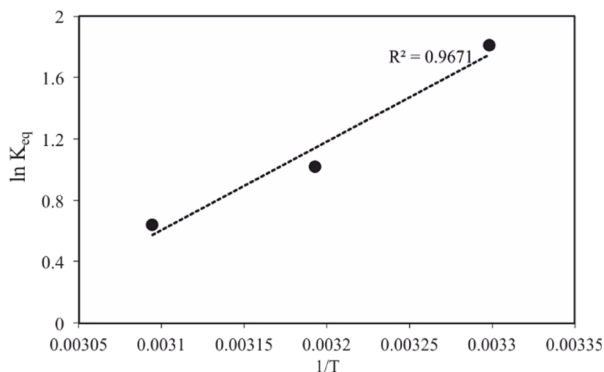
Fig. 9. Dependence of lnK_{eq} on $1/T$ (exothermic reaction)

The value of ΔH° decreased from ca. –56 to –35 kJ·mol^{-1} (on average ΔH° = –42.94 kJ·mol^{-1}) with an increase in temperature which shows an exothermic nature of adsorption. A high value of ΔH° points to the probable adsorption mechanism as chemisorption. Positive ΔS° (0.12 kJ·mol^{-1}·K^{-1}) confirms the increased randomness at the solid–liquid interface during adsorption. This is because of the increase of mobility of adsorbate ions/molecules in the solution with an increase in temperature.

Table 4

Thermodynamic parameters of MB adsorption onto WCS

ΔH [kJ·mol^{-1}]	ΔS [kJ·mol^{-1}·K^{-1}]	ΔG [kJ·mol^{-1}]		
		303 K	313 K	323 K
–42.94	0.12	–91.09	–92.52	–93.95

Gibbs free energy change (ΔG°, kJ·mol^{-1}) was calculated from:

$$\Delta G^\circ = \Delta H^\circ - T\Delta S^\circ \tag{18}$$

$\Delta G°$ in the examined temperature range varied ca. from –91 to –93 kJ·mol^{-1} (Table 4) which was well within the range of chemisorption (>40 kJ·mol^{-1}). $\Delta G°$ was negative and increased with increase in temperature which shows that the process is spontaneous and more favorable at a lower temperature.

4. CONCLUSIONS

WCS is an effective adsorbent for the removal of methylene blue. In this study, process optimization was carried out to obtain the highest efficiency. WCS showed the maximum adsorption efficiency at 5 g·dm^{-3} of adsorbent dose and pH 5–8. The Langmuir isotherm was the best fit ($R^2 = 0.998$) which shows that the adsorption is a monolayer with an adsorption capacity of 54.9 mg·g^{-1}. The adsorption process obeyed the pseudo-second order kinetic model. Chemisorption nature of the WCS adsorbent was confirmed through Langmuir and pseudo-second order best fits as well as the thermodynamic data. The MB adsorption at the solid-liquid interface was spontaneous and exothermic in nature under the studied conditions. The present study shows that WCS can be used as an efficient adsorbent for the removal of methylene blue dye from aqueous solution.

ACKNOWLEDGMENTS

REFERENCES

[1] DOD R., BANERJEE G., SAINI S., *Adsorption of methylene blue using green pea peels (Pisum sativum): A cost-effective option for dye-based wastewater treatment*, Bioproc. Eng., 2012, 17, 862.

[2] CHATTERJEE S., LEE D.S., LEE M.W., WOO S.H., *Congo Red adsorption from aqueous solutions by using chitosan hydrogel beads impregnated with nonionic or anionic surfactant*, Biores. Techn., 2009, 100, 3862.

[3] HAMEED B., *Grass waste: A novel sorbent for the removal of basic dye from aqueous solution*, J. Hazard. Mater., 2009, 166, 233.

[4] DEMIR H., TOP A., BALKÖSE D., ULKU S., *Dye adsorption behavior of Luffa cylindrica fibers*, J. Hazard. Mater., 2008, 153, 389.

[5] FERRERO F., *Dye removal by low cost adsorbents: Hazelnut shells in comparison with wood sawdust*, J. Hazard. Mater., 2007, 142, 144.

[6] MCKAY G., PORTER J., PRASAD G., *The removal of dye colours from aqueous solutions by adsorption on low-cost materials*, Water, Air, Soil Poll., 1999, 114, 423.

[7] KANNAN C., BUVANESWARI N., PALVANNAN T., *Removal of plant poisoning dyes by adsorption on tomato plant root and green carbon from aqueous solution and its recovery*, Desalination, 2009, 249, 1132.

[8] HAMEED B.H., *Evaluation of papaya seeds as a novel non-conventional low-cost adsorbent for removal of methylene blue*, J. Hazard. Mater., 2009, 162, 39.

[9] Bilal M., Shah J.A., Ashfaq T., Gardazi S.M.H., Tahir A.A., Pervez A., Haroon H., Mahmood Q., *Waste biomass adsorbents for copper removal from industrial wastewater. A review*, J. Hazard Mater., Part 2, 2013, 263, 322.

[10] Xue Q., Peng W., Ohkoshi M., *Molecular bonding characteristics of Self-plasticized bamboo composites*, Pakistan J. Pharm. Sci., 2014, 27, 975.

[11] Liu X., Zhu H., Qin C., Zhou J., Zhao J.R., Wang S., *Adsorption of heavy metal ion from aqueous single metal solution by aminated epoxy-lignin*, BioRes., 2013, 8, 2257.

[12] Zhang J., Chen H., Pizzi A., Li Y., Gao Q., Li J., *Characterization and application of urea-formaldehyde-furfural co-condensed resins as wood adhesives*, BioRes., 2014, 9, 6267.

[13] Pavia D., Lampman G., Kriz G., Vyvyan J., *Introduction to spectroscopy*, Cengage Learning P., 2007, 38.

[14] Shahul Hameed K., Muthirulan P., Meenakshi Sundaram M., *Adsorption of chromotrope dye onto activated carbons obtained from the seeds of various plants: Equilibrium and kinetics studies*, Arabian J. Chem., 2017, 10, S2233.

[15] Yu L., Luo Y.-M., *The adsorption mechanism of anionic and cationic dyes by Jerusalem artichoke stalk-based mesoporous activated carbon*, J. Environ. Chem. Eng., 2014, 2 (1), 220.

[16] Langmuir I., *The adsorption of gases on plane surfaces of glass, mica and platinum*, J. Am. Chem. Soc., 1918, 40, 1361.

[17] Freundlich H.M.F., *Over the adsorption in solution*, J. Phys. Chem., 1906, 57A, 385.

[18] Dubinin M.M., Radushkevich L.V., *Equation of the characteristic curve of activated charcoal*, Proc. Acad. Sci. USSR, Phys. Chem. Section, 1947, 55, 331.

[19] Temkin M., Pyzhev V., *Kinetics of the synthesis of ammonia on promoted iron catalysts*, Acta Phys. USSR, 1940, 12, 217.

[20] Aharoni C., Ungarish M., *Kinetics of activated chemisorption. Part 2. Theoretical models*, J. Chem. Soc., Faraday Trans. 1, Phys. Chem. Cond. Phases, 1977, 73, 456.

[21] Kumar P.S., Gayathri R., *Adsorption of Pb^{2+} ions from aqueous solutions onto bael tree leaf powder: Isotherms, kinetics and thermodynamics study*, J. Eng. Sci. Technol., 2009, 4, 381.

[22] Ahmaruzzaman M., Gayatri S.L., *Activated tea waste as a potential low-cost adsorbent for the removal of p-nitrophenol from wastewater*, J. Chem. Eng. Data, 2010, 55, 4614.

[23] Hameed B., Chin L., Rengaraj S., *Adsorption of 4-chlorophenol onto activated carbon prepared from rattan sawdust*, Desalination, 2008, 225, 185.

[24] Ho Y.S., Chiang T.H., Hsueh Y.M., *Removal of basic dye from aqueous solution using tree fern as a biosorbent*, Proc. Biochem., 2005, 40, 119.

[25] Rehman S., Adil A., Shaikh A.J., Shah J.A., Arshad M., Ali M.A., Bilal M., *Role of sorption energy and chemisorption in batch methylene blue and Cu^{2+} adsorption by novel thuja cone carbon in binary component system: Linear and nonlinear modeling*, Environ. Sci. Pollut. Res., 2018, 25, 31579.

[26] Ho Y.S., *Review of second-order models for adsorption systems*, J. Hazard. Mater., 2006, 136 (3), 681.